Research Article

SOHAG JOURNAL OF SCIENCES

https://doi.org/10.21608/sjsci.2024.248570.1149

Structural, Electrical, and Thermo-electric Characterization of Lightly Zn- doped PbS Films for NH_3-gas Sensing

E. Kh. Shokr[1], W. S. Mohamed[1,2], A. G. Adam[1,*], Moumen S. Kamel[3], H. M. Ali[1]

[1] *Physics Department, Faculty of Science, Sohag University, Sohag 82524, Egypt*
[2] *Physics Department, College of Science, Jouf University, Al-Jouf, P.O. Box 2014, Sakaka, Saudi Arabia*
[3] *Chemistry Department, Faculty of Science, Sohag University, Sohag 82524, Egypt*
**Email: ahmed.adam@science.sohag.edu.eg*

Received: 15th November 2023 **Revised:** 13th December 2023 **Accepted:** 1st January 2024
Published online: 30th January 2024

Abstract: The lightly Zn-doped $(PbS)_{1-x}$ $(Zn)_x$ with x=0, 0.03, and 0.05 wt.% in thin film form were produced by thermal vacuum evaporation. The structural, morphological, and elemental composition of the thin films has been analyzed using XRD, SEM, and EDXS, respectively. The electrical conductivity and Seebeck coefficient of $(PbS)_{1-x}$ $(Zn)_x$ film of 200 nm thick were determined and discussed. Thin films' electrical conductivity increased with temperature and film thickness. Pure PbS films manifested a positive Seebeck coefficient value indicating a P-type semiconducting behavior. The appearance of negative S values in Zn: PbS films could be assigned to the increase in electron concentration provided by Zn-doping and refers to the change of the conduction to n-type one. Pure films possess a high majority carrier concentration of 8.07×10^{18} Cm^{-3}. Zinc-metal-doped lead sulfide thin films were tested as NH_3 gas sensors with 150 ppm of target gas concentration. The sensitivity of the PbS sensor to NH_3 gas was determined at various gas concentrations ranging from 50 to 150 ppm. The gas sensitivity increased as concentrations increased. The best-attained results of 93% and 174s & 310s for sensitivity and response & recovery times respectively, were obtained by $(PbS)_{0.95}$ $(Zn)_{0.05}$ at RT.
Keywords: lead sulfide thin films, The parameters of the microstructure, thermal vacuum evaporation, and electrical conductivity, and Seebeck coefficient

1. Introduction

Gas sensors are important for many industrial applications, including process control, industrial health and safety, and environmental monitoring and detection **[1-3].** Ammonia emissions contribute significantly to the production of secondary inorganic aerosols **[4,5]**. Additional common sources of ammonia are soils, fertilizers, chemical manufacture, etc. It is obvious how important it is to find this gas.

PbS films were produced utilizing several procedures, such as chemical bath deposition (CBD), thermal evaporation deposition, spray pyrolysis, and deposition by electrochemistry, for use in contemporary applications **[6-8]**. For instance, all NH_3, NO_2, H_2S, water vapor, SO_2, CH_3OH, LPG, benzene, CH_3COCH_3, HCHO, and CCl_4 gases demonstrate a gas response based on their resistivity **[2].**

PbS is a highly good and widely used optoelectronic semiconducting semiconductor. PbS is used in gas sensing applications because of its ability to detect changes in material resistance in response to various gaseous atmospheres. This change is caused by the interchange of charge carriers between the surface of the sensor material and the absorbed gas. Therefore, the surface structure of PbS would dictate its gas-sensitive characteristics.

PbS is a significant IV-VI compound semiconductor having a small band gap that has found widespread use in optical communication apparatus, radiation-detecting devices, and optical data storage due to its unique optoelectronic features **[9-11]**. Additionally, the excitation Bohr radius of PbS is considerable (18 nm). It has a wide range of applications, including near-infrared sensors **[12,13]**, the indicators of biology **[14,15]**, materials with thermoelectric properties **[16]**, environmental applications **[17]**, quantum dot-based solar cells **[18]**, and solar cells of the third generation **[19-22].**

The interchange of charge carriers between the sensor material (PbS) and the adsorbed gas molecules (NH_3) might be related to the PbS gas sensing mechanism, leading to a modification in the sensor's resistance conductivity **[23].**

In the present paper, thermal vacuum deposition was used to prepare $(PbS)_{1-x}(Zn)_x$ (x=0, 0.03 and 0.05) thin films. Investigations were conducted to determine how Zn doping affected the films' microstructural, morphology, electrical, Seeback, and gas sensor characteristics of the films under study. Following that, novel characteristics of thin films are acquired for NH_3 gas sensor applications.

2. Experimental details

2.1 Thin Film Synthesis

Undoped and zinc metal-doped lead sulfide thin films with a thickness of 200 nm have been prepared on glass slides with the Edwards E306A coating equipment and the thermal evaporation method. The rate of deposition showed a change from 1.2 to 3.5 Å/sec as we were preparing our films. At the beginning of the deposition step, the chamber was evacuated to 4×10^{-4} mbar and 3.63×10^{-5} mbar at its final stage. High-purity 99.99% lead sulfide (PbS) and zinc (Zn) powders from the Aldrich Association were employed to obtain the produce samples. The

powder mixes of $(PbS)_{1-x}$ $(Zn)_x$ (where x = 0, 0.03 and 0.05 wt.%) were synthesized using stoichiometric quantities of high purity of Zn and PbS. Cold pressing was used to form the product into tablets. To obtain uniformity in the compounds. The samples are combined and heated for two hours at 300 ℃, three hours at 350 ℃, and two hours at 400 ℃. After re-milling the samples for two hours, the powder that was produced was pressed into tablets. The tablets went through a sintering process at a temperature of 600℃ for three hours to obtain the uniformity of the forming compounds utilized as our thin film sources. The tablets were put inside a molybdenum vessel which possessed a melting point of around 2600 °C.

The substrates were cleaned in an ultrasonic cleaner (VGT-1613 QTD) equipped with an electronic timer that could contain 2000 mL after initially being cleaned with acetone and hot distilled water. The INFICON model digital film thickness meter, namely the SQM-16, was utilized to determine the thickness of the film and the rate of the thermal deposition process.

2.2. Thin Film Characterizations

The X-ray diffractometer (XRD) method was employed for analyzing the structural characteristics of $(PbS)_{1-x}$ $(Zn)_x$ (where x = 0, 0.03 and 0.05 wt.%). The XRD measurements were carried out using a German Bruker D8 Advance device. Copper (Cu) was utilized as the target material, while nickel (Ni) was used as the filter. The copper kα1 radiation with a wavelength of 1.54 Å was employed as the X-ray source. The XRD measurements were carried out at a scan rate of 2.6 degrees per minute (°/min) with an operating voltage of 30 kV and a current of 30 mA.

The surface morphology and chemical composition of $(PbS)_{1-x}$ $(Zn)_x$ films were studied using field emission scanning electron microscopy (FE-SEM). The analysis was investigated with a JSM-6100 microscope made in Japan by JEOL. The chemical compositions of the films were examined using the Energy Dispersive X-ray Spectroscopy (EDS) unit (HNU5000, USA) with the FE-SEM.

In the temperature range of 450–670 K, we used a two-point probe approach to evaluate the electrical resistance of the samples. Two electrodes were formed on the samples using a silver paste, spaced approximately 2 mm apart, with no silver paste in the middle of the films. The electrometer device (HP HEWLETT-PACKARD) and a chromel-alumel thermocouple were employed to measure the specimen's resistance and temperature, respectively.

The Seebeck coefficient was determined for a 200 nm thick film of $(PbS)_{1-x}(Zn)_x$ that was deposited on glass slides at RT. Using this formula to determine the kind of carriers and have a better knowledge of the conducting behavior.

$$S = \frac{\Delta V}{\Delta T} \quad (1)$$

where S is the Seebeck coefficient at RT. The sample's seeback voltage was measured with a digital micro voltmeter, and the temperature was measured with a thermal contact chromel-alumel thermocouple on the surface of the specimen.

$(PbS)_{1-x}(Zn)_x$ samples with a thickness of 200 nm deposited on glass slides were experimentally evaluated as NH_3 gas sensors. The sensor was mounted inside a closed container of plastic containing various concentrations of NH_3. When the sensor was exposed to NH_3, its resistance increased for pure PbS and decreased for Zn-doped PbS, indicating the sensor's highly sensitive samples and quick response to NH_3

3. Results and Discussion:

3.1. Structural analysis

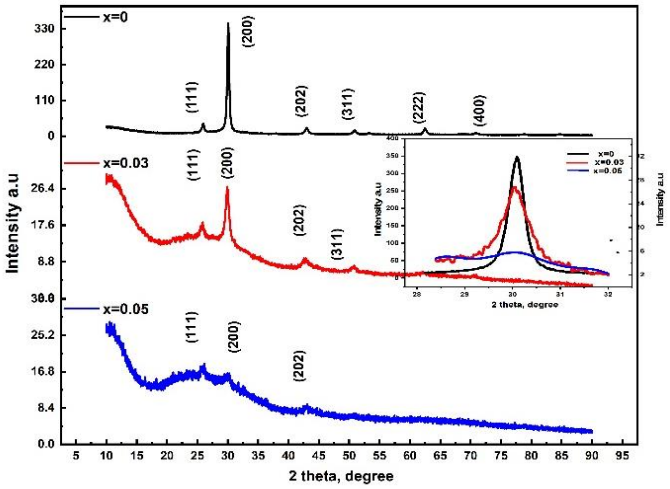

Fig. 1: XRD spectrum of $(PbS)_{1-x}Zn_x$ (x=0, 0.03 and 0.05) thin films of 200 nm thick

Figure 1 shows the Zn: PbS XRD patterns for x = 0, 0.03, and 0.05 wt%. As can be seen, all peaks for the undoped film (x = 0) relate to the PbS, indicating a high degree of purity of the film. Furthermore, with Zn-doped films, the Zn element could not be represented by any phases, suggesting that Zn was effectively incorporated into the PbS lattice. The intensity of the observed peaks and the number of peaks decrease as the Zn-doping ratio increases, showing an increase in microstructural disorder **[23].** For undoped PbS, some observed peaks at 2θ =25.97, 30.084, 43.064, 50.984, 53.426 and 62.535 are corresponding to (111), (200), (202), (311), (222) and (400), respectively, compatible with standard data JCPDS COD 9008694.

In the F.C.C. cubic structure, crystalline growth has a preferred direction along the most intense peak (200). As shown in Fig. 1 and Table 1, the drop in β-values with doping indicates that Zn-doping leads to peak broadening and intensity reduction. The following equations are used to estimate the crystallite size D, lattice strain ε, dislocation density δ, lattice constant a, and d-spacing, respectively.

$$D = \frac{0.94\,\lambda}{\beta \cos\theta} \quad (2)$$

$$\varepsilon = \frac{\beta \cos\theta}{4} \quad (3)$$

$$\delta = \frac{1}{D^2} \quad (4)$$

$$a = d\sqrt{h^2 + k^2 + l^2} \quad (5)$$

$$d = \frac{\lambda}{2sin\theta} \quad (6)$$

Under these conditions, β stands for the overall width at half-maximum of the XRD peak, θ for Bragg's angle, and λ for the X-ray wavelength.

Table 1 shows that the crystallite size D decreases with Zn doping, which is typical of substitutional doping [24-26]. Because doped Zn has a smaller (0.74 Å) ionic radius than Pb2+ (1.19 Å), it is easier for it to occupy substitutional sites in the PbS lattice, resulting in a shrinkage in crystalline size, a fact verified by the detected peak shift to lower θ values causing a $cos\theta$ increase (equ 1).

Equations 1-3 indicate a rise in both and with increasing doping levels, which may be related to the formation of defects in the lattice structure. The parameters of the microstructure of the films displayed in Table 1 confirm that the crystallite size decreases as the Zn dopant concentration increases. Additionally, an increasing tendency for lattice defects such as internal microstrain and dislocation density may be observed with an increase in Zn dopant. Such a change may be caused by the crystalline degradation nature [27].

Equations 4 & and 5 explain the observed increases in cell volume (V= a 3), lattice constant, and d-spacing as the (200) peak shifts to a lower 2θ value.

Table1. The parameters of the microstructure of the Zn: PbS films of preferable (2 0 0) Orientation.

X (Wt %)	2 ɵ (deg.)	β (deg.)	D (nm)	ε×10^{-3}	δ× 10^{12}cm^{-2}	d spacing (Å)	a (Å)	V (Å^3)
0	30.08	0.36	23.86	1.52	0.176	2.97	5.94	209
0.03	29.9	0.93	9.23	3.92	1.17	2.98	5.96	211
0.05	30.07	0.97	8.85	4.08	1.28	2.96	5.92	207

3.2. Morphological analysis (SEM)

Fig.2 shows the microstructures and surface morphologies of $(PbS)_{1-x}(Zn)_x$ thin films with different concentrations. The grains are found to be homogeneously spread and highly collected on the film surface, with an aptitude for spherical shapes. The size of grains is not uniform [28] and the grain size varies with the amount of Zn concentration. The mean particle sizes determined by the J-programme ranged from 70 to 188 nm.

3.3.Compositional analysis (EDXS)

The chemical compositions of the present samples with a composition of Zn: PbS were analyzed using EDXS, as shown in Fig.3. The appeared signals correspond to Pb, S, and Zn, and no other signals can be identified for contaminants or impurities that accomplish the subject films. A random variation in the Pb:S ratio that appeared in the spectra could be owing to the effect of surface roughness or the existence of a few inherent defects inside the films [29] because of the deficiency of sulfur during the thermal deposition of the film [30,31].

3.4. Electrical Properties

Figure 4 illustrates the temperature effect on the electrical conductivity of Zn: PbS thin films, it is obvious that the electrical conductivity value of the films increases with the Zn doping increase, which can be related to the increase in carrier concentration due to substitutional incorporation of Zn ions in the PbS structure and/ or sulfur deficiencies [30,31]. This Sulfur release can occur during the thermal deposition process and leads to an excess of Pb atoms that act as donor single sites.

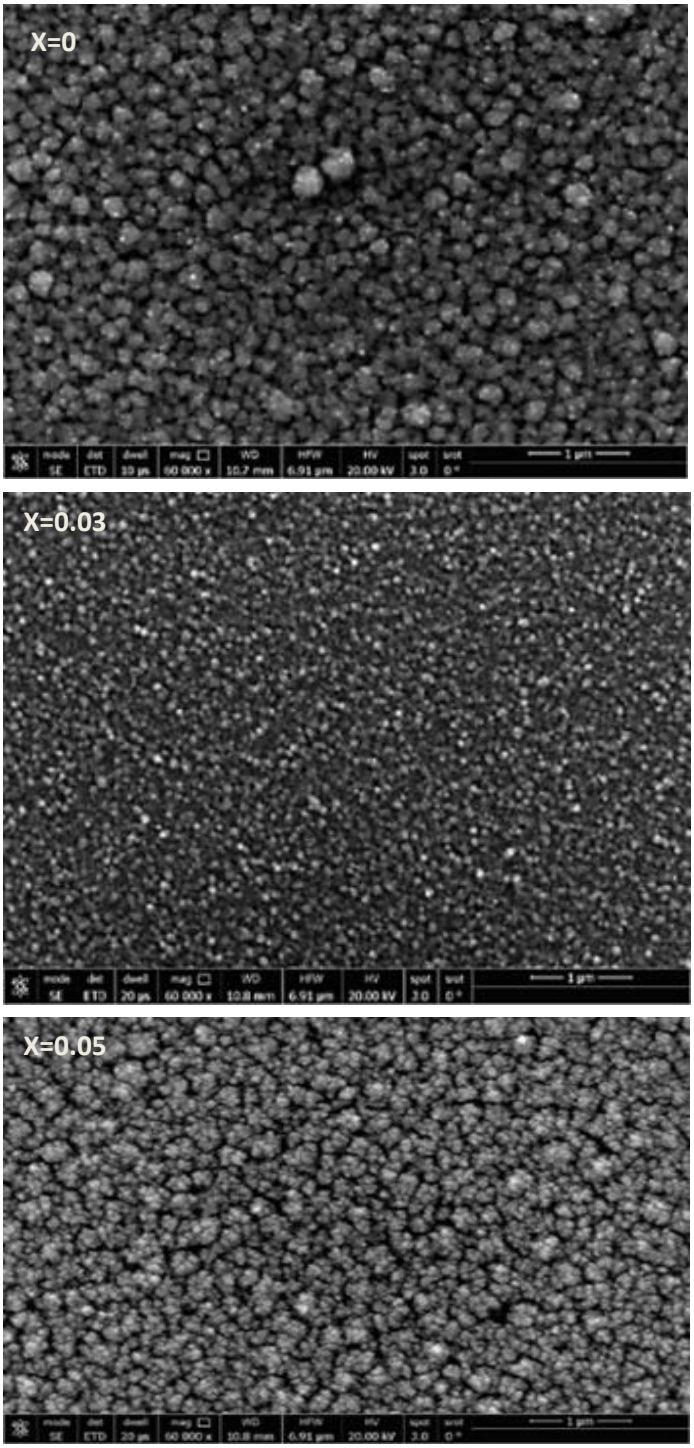

Fig.2: SEM images of $(PbS)_{1-x}Zn_x$ deposited on a glass

Besides, conductivity activation by the increase in

temperature indicates the semiconducting behavior of the films. The thermal activation energy E_σ can be computed using the following Arrhenius relation:

$$\sigma = \sigma_1 \exp(\frac{-E_{\sigma 1}}{k_B T}) + \sigma_2 \exp(\frac{-E_{\sigma 2}}{k_B T}) \quad (7)$$

The symbols $E_{\sigma 1}$ and $E_{\sigma 2}$ represent the thermal activation energies associated with conductions, where σ_1 and σ_2 are the pre-exponential factors wthatexhibits variability in its values based on the specific type of conductivity, k_B is Boltzmann's constant and T is the absolute temperature. The well-fitting to straight portions of ln (σ) with 1000/T plots are illustrated in Fig.5

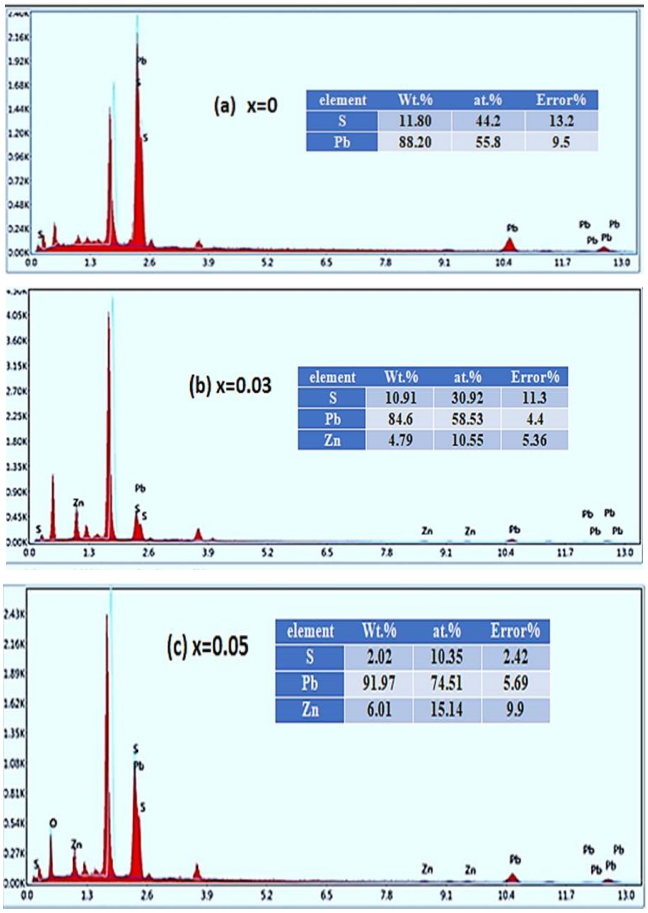

Fig. 3. EDXS of $(PbS)_{1-x}Zn_x$ at x=0 (a), x=0.03 (b), and x=0.05 (c) deposited on glass slides

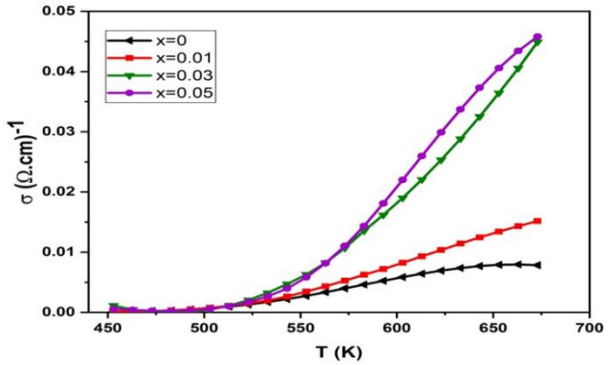

Fig.4. (σ)-(1000/T) for different compositions of $(PbS)_{1-x}$ Zn_x film with 200 nm thick

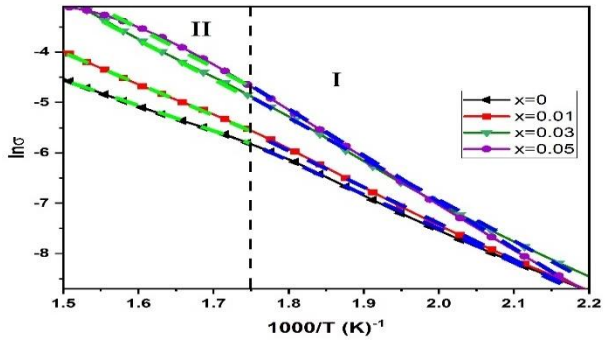

Fig. 5. ln(σ) - (1000/T) for different compositions of $(PbS)_{1-x}$ Zn_x film with 200 nm thick

The type of conduction in the films can be identified by the polarity and values of the Seeback coefficient S, Table 2. The positive S value of the pure PbS film illustrates its P-type semiconducting behavior. The negative values of S appeared for Zn: PbS films refer to the transformation of the conduction to n-type one. Such results of S could be described by the following two opposite carrier mechanisms [32]:

$$S = \frac{|S_p|\mu_p p - |S_n|\mu_n n}{\mu_p p + \mu_n n} = \frac{|S_p| - |S_n|\frac{\mu_n n}{\mu_p p}}{1 + \frac{\mu_n n}{\mu_p p}} \quad (8)$$

According to the mentioned P-to-n-type transition, can take place when $\frac{\mu_n n}{\mu_p p}$ the ratio is larger enough than unity due to the increase in mobility value and/or the electron density offered by Zn-doping.

Besides to Benko and Koffy [33], the Seebeck coefficient is associated with the energy position E_f of Fermi-level through the following relation:

$$\frac{E_f}{K_T} = \frac{|S|e}{K} - A, \text{where} A \approx 1. \quad (9)$$

For P-type semiconductors, the negative and positive values of E_f refer to degenerate and non-degenerate semiconductors, respectively, and vice versa for n-type ones. Thus, from the values of $e^{\frac{E_f}{KT}}$ recorded in Table .2, one can conclude that the P-type PbS film is a degenerate semiconductor, but all Zn-doped films are non-degenerate semiconductors. The concentrations of the majority charges (N) at room temperature in the considered films were calculated using the following equation;

$$N = \frac{2(2\pi mKT)^{3/2}}{h^3} e^{Ef/KT} \quad (10)$$

and recorded in Table.2. The N-values confirm the degenerate and non-degenerate behaviors of pure and Zn-doped films, respectively.

3.5 NH_3 Gas sensing

The adsorbed environmental oxygen molecules on the n-type film surface acting as acceptor centers trap electrons from the material forming a negatively charged layer on the surface, where O_2 ads+$2e^- \rightarrow 2O^-$ this leads to the majority charge carriers (electrons) concentration decreasing. Therefore, the n-type Zn: PbS resistance films increase and may become overloaded at RT. However, for P-type PbS films, the trapped electrons by oxygen molecules make the hole concentration ratio more

significant in the film, causing a resistance decrease to a certain relatively low value at RT.

Table 2. The characteristics of the seeback coefficients of the $(PbS)_{1-x}$ Zn_x films

x(wt%)	$\Delta E_{\sigma 1}$	$\Delta E_{\sigma 2}$	S (V/K)	E_f/K_T	e^{Ef}/K_T	N(cm^{-3})
0	0.44	0.57	+0.000008	-0.907	0.403663	8.07×10^{18}
0.01	0.54	0.62	-0.000743	-9.62	6.63×10^{-5}	1.33×10^{15}
0.03	0.68	0.70	-0.0007	-9.12	0.000109	2.18×10^{15}
0.05	0.56	0.79	-0.00067	-8.77	0.000155	3.09×10^{15}

When the n-type or P-type films are exposed to reducing NH_3-gas, which reacts with oxygen ions liberating the electrons back to the films, where

$$2NH_3 + 7O^-(ads.) \rightarrow 3H_2O + 2NO_2 + 7e^- \quad (11)$$

These liberated electrons enlarge the electron density in n-type Zn:PbS films lowering their resistances, while they recombine with the holes in P-type PbS film reducing their concentration and consequently the film resistance increases. Such impact of NH_3 on the electrical resistance of PbS and Zn: PbS films has been exploited for NH_3-gas sensing.

The performance of the gas sensing process was evaluated through the following indicating parameters:

1-Sensitivity(S): which is the minimum concentration of the target gas that can be detected. It can be expressed by the following relation **[34]** .

$$S = |R_{in} - R_g|/R_g \quad (12)$$

where R_{in} and R_g are the initial and after gas exposure, respectively.

2- Reversibility: the sensor's ability to restore its original state.

3- Response time (tres): the sensor's necessary time to identify the target gas, which is estimated by the time necessary to attain 90% of the complete variations during the response process **[35,36].**

4- Recovery time (t_{rec}): the sensor's necessary time for the sensor to attain 90% of the complete variation during the recovery process.

Figure. 7 (a,b) gives the resistance variation of the present films with NH_3 exposure time (texp) about the Zn-doping ratio and gas concentration. As shown, the resistance of the undoped or Zn-doped PbS films increases or decreases with the elongation of texp attaining its maximum or minimum values at texp= 500 or 400 sec, respectively.

After ending the gas exposure towards the p-type-PbS or n-type Zn: PbS films, the resistance decreases or increases attaining, its initial value Rint within a certain recovery time trec depending on the gas concentration or Zn-doping ratio, respectively. This confirms the reversibility of the NH_3 gas-sensing process of the present films.

Figure 8 (a) depicts the sensitivity variations with gas exposure time texp at different gas concentrations and Zn-dopant ratio. As shown, S increases with either gas concentration increase or exposure time elongation to its saturation value at texp ≥300 sec. Besides, both response tres and recovery trec times were calculated and noted in Table 3.

As seen in Fig.8 (b), S begins to slightly increase and after a certain period of gas exposure depending on Zn-doping level it abruptly increases attaining, its maximum value, Smax of 73, 91,93 % at texp=360, 381 & 400 sec for $(PbS)_{1-x}Zn_x$ films of x=0.01, 0.03 & 0.05, respectively, and then declines with further elongation of texp.

This decline in S-values may be assigned to the increase in R_g-values with texp elongation because of the density decrease or maybe exhausting of the surface adsorbed oxygen molecules, which results in the reduction or even ending of the liberated electrons back to the n-type Zn: PbS sensor material. The S-texp behavior could be more clarified by employing the sensitivity variation rate given by

$$the\ the\ \frac{dS}{dt_{exp}} = \frac{R_{init}}{R_g{}^2}\left(\frac{dR_g}{dt_{exp}}\right) \quad (13)$$

indicates that S-variation is proportional to $R_g{}^{-2}$ values and $\frac{dR_g}{dt_{exp}}$ trend.

Table.3 summarizes the obtained NH_3 sensing results compared with some reported ones. The obtained results of 91%, 120 sec &630 sec and 93%, 174 sec & 310 sec of sensitivity response and recovery times, respectively, for zinc-doped films were better than those of un-doped lead sulfide film.

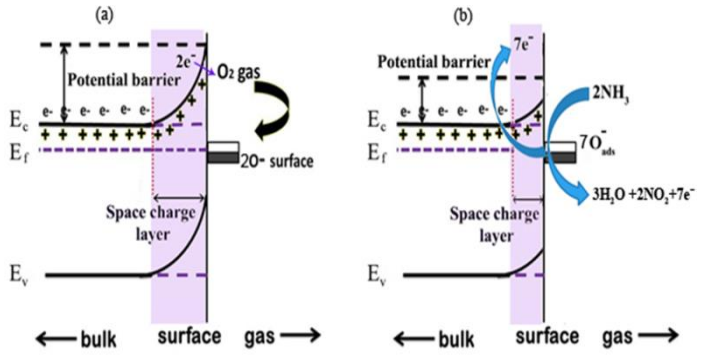

Fig. 6: NH_3 sensing operation by n-type semiconductor. (a) effect of environmental oxygen, (b) after NH_3 adsorption

Conclusions

Thin films of lead sulfide doped with zinc have been produced through the thermal evaporation method. The film's structural investigation by x-ray diffraction showed that the intensities of the observed PbS peaks and the number of crystalline peaks decreased with the increase in Zn doping levels, indicating an increase in microstructural disorder. SEM measurements manifest that the grains are found to be spread and highly collected on the film surface,with an aptitude for spherical shapes. The chemical compositions of the present samples with a composition of Zn: PbS were analyzed using EDS, showing the deficiency of sulfur during the thermal deposition of the film which impacted the film conductivity.

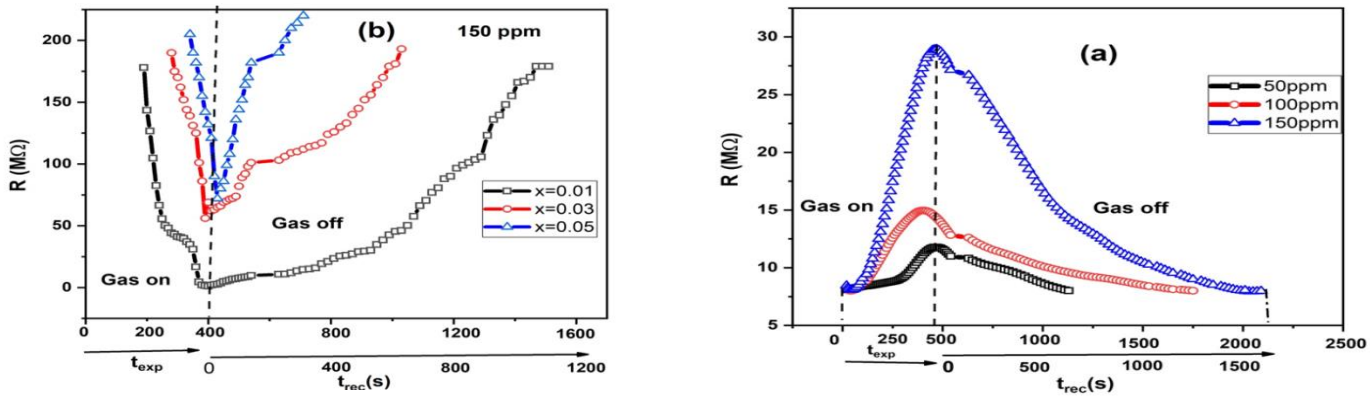

Fig. 7. The response of $(PbS)_{1-x}$ Zn_x where x=0.01, 0.03 and 0.05 W.t% sensor resistance towards NH_3 with time at different concentrations (50, 100 and 150 PPm).

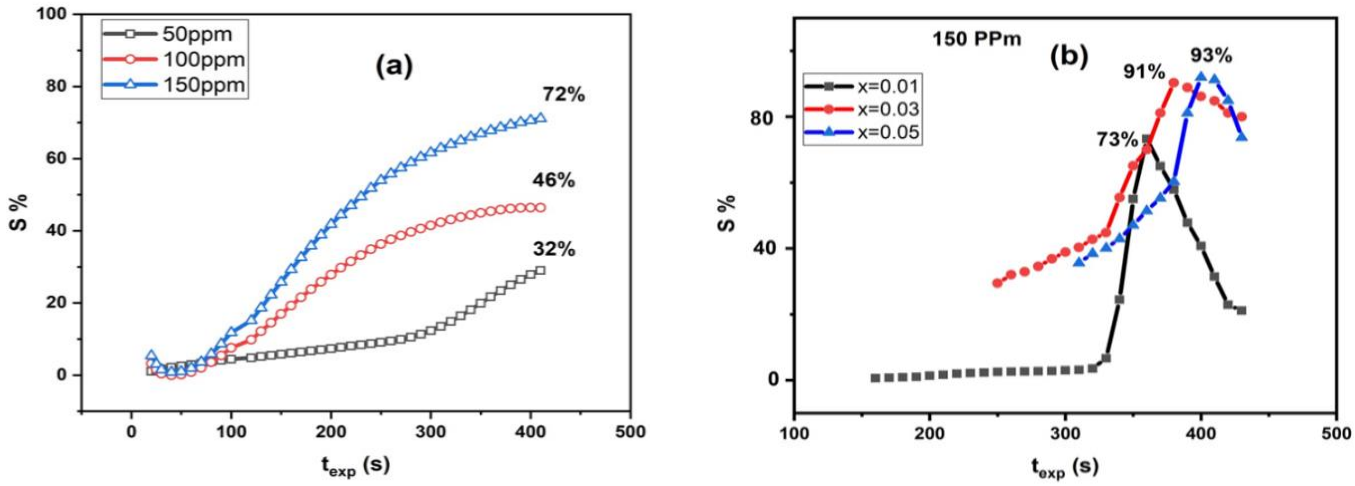

Fig. 8. Change of $(PbS)_{1-x}Zn_x$ where (a) x=0 and (b) x=0.01, 0.03 and 0.05 W.t% sensitivity with $time_{exp}$ at various concentrations

Table 3 comparision of the present results with the earlier publications of PbS thin films as NH_3 gas sensors**.**

X (wt%)/	Deposition method	Sensor concentrations	$R_{init}(\Omega)$	S%	t_{res}(S)	t_{rec} (S)	Ref
X=0	Thermal evaporation	50	8×10^6	32	330	735	Present Work
		100	8×10^6	46	223	1340	
		150	8×10^6	72	292	1650	
X=0.01		150	178×10^6	73	23	1100	
X=0.03			190×10^6	91	120	630	
X=0.05			205×10^6	93	174	310	
PbS	PbS prepared with Na2S used for precipitating agent	301	-	8.08	46	67	[37]
PbS nanostructures	Chemical precipitation.	120	90	26	60	--	[38]
PbS nanostructures	Sol-gel technique	0.22	-	7.3	52	70	[2]
perovskite halide $CH_3NH_3PbI_3$ (MAPI)	standard method	1	-	55	140	120	[39]
polyaniline/SrGe4O9	situ chemical oxidation polymerization method	0.2	-	95.1	62	223	[40]

The electrical conductivity measurements of $(PbS)_{1-x}Zn_x$ thin film of 200 nm thick deposited on glass slides confirmed a better knowledge of the conducting behavior. Seebeck coefficient study at RT demonstrated the p- to n-type behavior transition influenced by the Zn metal doping. $(PbS)_{1-x}Zn_x$ films investigation for gas, sensing has shown their good responses towards NH_3-gas where their sensitivity increases with target gas concentration increase. The best NH_3 sensing promise has appeared by $(PbS)_{0.95}Zn_{0.05}$ film of 200 nm at 150ppm of the gas according to its best results of 93% and 174 s & 310 s for sensitivity and response & recovery times respectively, while the sensitivity of PbS reaches only the maximum value of 72% at 150 ppm.

CRediT authorship contribution statement:

Conceptualization, methodology, software, validation, formal analysis, investigation, resources, writing—original draft preparation, project administration E. Kh Shokr, A.G.Adam; data curation, project administration, software, W.S.Mohamed, Moumen S. Kamel; writing—review and editing, supervision, visualization H. M. Ali. All authors have read and agreed to the published version of the manuscript.

Data availability statement

The data used to support the findings of this study are available from the corresponding author upon request.

Declaration of competing interest

The authors declare that they have no known competing financial interests or personal relationships that could have appeared to influence the work reported in this paper.

Acknowledgments

The author expresses gratitude to Sohag University for supporting this research

References

[1] S. T. Navale, D. K. Bandgar, M. A. Chougule and V. B. Patil, *RSC Adv*, 5(2015) 6518.
[2] S. Bandyopadhyay, *Particulate Science and Technology*, 30(2012) 43–54,
[3] V. V. Burungale, R.S. Devan, S.A.Pawar, N.S. Harale,V.L. Patil, V.K. Rao, Y. R.Ma, J.E. Ae, J.H.Kim, P.S. Patil, *Materials Science-Poland*, 34(2016), 204-211
[4] G. Huyberechts, M. Van Muylder,M. Honor'e, J. Desmet, J. Roggen, *Sens. Actuators B*, 18–19 (1994) 296–299.
[5] H. Xin, Y. Liang, A. Tanaka, R.S. Gates, E.F. Wheeler, K.D. Casey, K.D. Heber, J.Q. Ni, H. Li, *Proceedings of the Third International Conference on Air Pollution from Agricultural Operations, NC*, 12-15(2003)106.
[6] E. Pentia, L. Pintilie, I. Matei, T.Botila, E.Ozbaya, *J.Optoelectron.Adv. Mater*, 3(2001)525–530.
[7] S. Kumar, T.PSharma, M.Zulfequar, M.Husain,*Phys.B:Conden. Matter*, 325(2003)8–16.
[8] B. Thangaraju, P.Kaliannan, *Semicond.Sci.Technol*,15(2000)849–853.
[9] N.R. Mathewsa, C.Ángeles–Chávez, M.A.Cortés-Jácome, J. A. Antonio, Electrochim. Acta, 99(2013)76–84.
[10] Y. Zhou, H. Itoh, T. Uemura, K. Naka and Y. Chujo, *Langmuir*, 18(2002)5287.
[11] X. h. Yang, Q. S. Wu, Y. P. Ding and J. k. Liu, *Bull. Korean Chem. Soc*, 27 (2006)377.
[12] J.D. Patel, F. Mighri, A. Ajji, S. Elkoun, *Mater. Sci. Appl*, 3(2012)125–130.
[13] Z. Sun, Z. Liu, J. Li, G. Tai, S.P. Lau, F. Yan, *Adv. Mater*, 24 (2012) 5878–5883
[14] K. Hanaki, A. Momo, T. Oku, A. Komoto, S. Maenosono, Y. Yamaguchi, *Biochem. Biophys. Res. Commun*, 302(2003)496–501.
[15] F. Pinaud, X. Michalet, L.A. Bentolila, J.M. Tsay, S. Doose, J.J. Li, *Biomaterials*, 27(2006)1679–1687
[16] J.M. Skelton, S.C. Parker, A. Togo, I. Tanaka, A. Walsh, *Phys. Rev. B*, 89(2014)205203.
[17] M. Li, X. Wang, H. Ruan, Q. Zhang, Z. Wu, Y. Liu, Z. Lu, J. Hai, *J. Alloys Compd*, 768 (2018) 399e406.
[18] J. Tang, L. Brzozowski, A.D.R. Barkhouse, X. Wang, R. Debnath, R. Wolowiec, *ACS Nano*, 4 (2010) 869–878.
[19] J.M. Luther, J. Gao, M.T. Lloyd, O.E. Semonin, M.C. Beard, A.J. Nozik, *Adv. Mater*, 22 (2010) 3704e3707.
[20] C.-H.M. Chuang, P.R. Brown, V. Bulovi_c, M.G. Bawendi, *Nat. Mater*, 13 (2014) 796.
[21] H.A. Mohamed, *Solar Energy*,108(2014)360–369.
[22] B. Ding, T.Gao, Y.Wang, D.H.Waldeck, P.W.Leu, J.Lee, *Sol.Energy Mater. Sol.Cells*, 128(2014)386–393.
[23] E. Kh. Shokr , W. S. Mohamed, A. G. Adam , and H. M. Ali1, *J Mater Sci: Mater Electron*, 34 (2023)1929
[24] N. Neto, Y. Oliveira, C. Paskocimas, M. Bomio, F. Motta, *J. Mater. Sci*, 29 (2018) 19052
[25] A. Nakrela, N. Benramdane, A. Bouzidi, Z. Kebbab, M. Medles, C. Mathieu, *Results Phys*, 6 (2016)133
[26] N.F.A. de Neto, O.B. de Medeiros Ramalho, H. Fantucci, R.M. dos Santos, M. Bomio, F.V. da Motta, *J. Mater. Sci*,31(2020) 14192
[27] E Sarica, V Bilgin, *Materials Science in Semiconductor Processing* 68(2017)288 .
[28] B P Singh, RKumar, AKumar and RCTyagi, *Mater. Res. Express*, 2(2015) 106401
[29] Sat Kumar, Shushant Kumar Singh, Rakesh Kumar, Beer Pal Singh, *Journal of Materials Science & Surface Engineering*, 5(2017)500-503
[30] V. T. Sivaraman, S. V. Nagarethinam, R. A. Balu, *Progress in Natural Science: Materials International*, 25(2015)392-398
[31] S. Ravishankar, A. R. Balu, *Surface Engineering*, 33 (2017)506-511
[32] E Kh Shokr, *Semicond. Sci. Technol*, 15 (2000) 247–253.
[33] F.A. Benko, F.P. Koffyberg, *Solid State Communications*, 57(1986) 901-903
[34] Lei Sheng, Chen Dajing and Chen Yuquan, *Nanotechnology*, 22(2011)265504
[35] Shulin Yang, Zhen Chen, Zhao Wang, Gui Lei, Juan Xiong, Huoxi Xu, Haoshuang Gu, *Sensors and Actuators B: Chemical*, 367(2022)132026
[36] Y. Han, Y. Ma, Y. Liu, S. Xu, X. Chen, M. Zeng, N. Hu, Y. Su, Z. Zhou, Z. Yang, *Appl. Surf. Sci*, 493 (2019) 613–619.
[37] T. Fu, *Sensors and Actuators B*, 140 (2009) 116–121

[38] H.Karami1, M.Ghasemi, S.Matini, *Int. J. Electrochem. Sci*, 8(2013) 11661 – 11679
[39] A. Maity, A. K. Raychaudhuri & B. Ghosh, *Scientific reports*, 9(2019) 7777
[40] Yajie Zhang 1, Junxin Zhang 1, Yadong Jiang, Zaihua Duan, Bohao Liu, Qiuni Zhao, Si Wang, Zhen Yuan, Huiling Tai, *Sensors and Actuators B: Chemical*, 319(2020) 128293